Journal of
Composites Science

MDPI

Article

Shear Behavior and Modeling of Short Glass Fiber- and Talc-Filled Recycled Polypropylene Composites at Different Operating Temperatures

Andrea Iadarola [1,*], Pietro Di Matteo [2], Raffaele Ciardiello [1], Francesco Gazza [3], Vito Guido Lambertini [3], Valentina Brunella [2] and Davide Salvatore Paolino [1]

[1] Department of Mechanical and Aerospace Engineering, Politecnico di Torino, C.so Duca degli Abruzzi 24, 10039 Turin, Italy; raffaele.ciardiello@polito.it (R.C.); davide.paolino@polito.it (D.S.P.)
[2] Department of Chemistry, Università degli Studi di Torino, Via Pietro Giuria 7, 10125 Turin, Italy; pietro.dimatteo@unito.it (P.D.M.); valentina.brunella@unito.it (V.B.)
[3] Material Technical Expertise Department, Centro Ricerche Fiat (Stellantis), C.so Giovanni Agnelli 220, 10135 Turin, Italy; francesco.gazza@crf.it (F.G.); vitoguido.lambertini@crf.it (V.G.L.)
* Correspondence: andrea.iadarola@polito.it

Abstract: The present paper aims to broaden the field of application of the phenomenological model proposed by the authors in a previous study (ICP model) and to assess the shear properties of a recycled 30 wt.% talc-filled polypropylene (TFPP) and a recycled 30 wt.% short glass fiber-reinforced polypropylene (SGFPP), used in the automotive industry. The materials were produced by injection molding employing post-industrial mechanical shredding of recycled materials. In particular, Iosipescu shear tests adopting the American Standard for Testing Materials (ASTM D5379) at three different operating temperatures (−40, 23 and 85 °C) were performed. The strain was acquired using a Digital Image Correlation (DIC) system to determine the map of the strain in the area of interest before failure. Lower operating temperatures led to higher shear chord moduli and higher strengths. Recycled SGFPP material showed higher mechanical properties and smaller strains at failure with respect to recycled TFPP. Finally, the ICP model also proved to be suitable and accurate for the prediction of the shear behavior of 30 wt.% SGFPP and 30 wt.% TFPP across different operating temperatures.

Keywords: Iosipescu; mechanical tests; polymers; recycled materials; automotive

Citation: Iadarola, A.; Di Matteo, P.; Ciardiello, R.; Gazza, F.; Lambertini, V.G.; Brunella, V.; Paolino, D.S. Shear Behavior and Modeling of Short Glass Fiber- and Talc-Filled Recycled Polypropylene Composites at Different Operating Temperatures. *J. Compos. Sci.* **2024**, *8*, 345. https://doi.org/10.3390/jcs8090345

Academic Editor: Zhong Hu

Received: 23 July 2024
Revised: 20 August 2024
Accepted: 27 August 2024
Published: 3 September 2024

1. Introduction

In the automotive industry, plastic usage has been constantly rising since the 1950s; this growth appears even more relevant when expressed in terms of a percentage of car weight [1]. Given the large amount of polymers present in cars and the increasing attention afforded to the sustainability of new vehicles [2], the use of recycled materials has become a fundamental aspect of the automotive industry in saving raw materials and reaching sustainable goals. In particular, the usage of recycled composite materials is considered one of the best solutions to reduce carbon emissions and fuel consumption or increase battery autonomy by reducing the weight of vehicles. These materials can offer comparable or even better specific mechanical properties when compared to the most used materials in cars, such as steel or aluminum [3].

In recent years, several approaches have been adopted for recycling thermoplastic composites [4]; among them, the most common are pyrolysis [5], solvolysis [5] and mechanical shredding [6]. In the case of low-cost fiber reinforcements, such as glass fiber-reinforced polymers (GFRP), the recycling processing method must not be expensive. For this reason, since mechanical shredding is the cheapest methodology, this process is typically adopted for producing such kinds of recycled polymer composites [7,8]. The adopted recycling

process can also have a key role in the resultant mechanical properties of the recycled polymer composite. Indeed, the mechanical behavior of short-fiber or mineral-filled polymers depends on many factors, such as the aging of the polymer, the radius of the reinforcement and its aspect ratio [9], fiber orientation [10], production process parameters [11], the strain rate and the operating temperature [12–14].

For this reason, knowledge and modeling of the tensile and shear behavior of recycled plastics are of prime importance when designing polymer components. In particular, concerning the shear behavior of materials, the Iosipescu test method [15] is the most used since it applies a uniform shear stress state to the specimens, it is relatively simple and reproducible, and it is not restricted to specific materials [16,17].

Concerning the tensile behavior of polymer composites, an abundance of data and phenomenological models are available in the literature. By contrast, the literature on the shear testing and phenomenological modeling of the shear behavior of recycled thermoplastic polymers is scarce, but there are some studies on non-recycled polymers with variants of Iosipescu [15] fixtures [18–21] and others [14,17].

Indeed, in 2006, Xiao [19] implemented a physically based model (CODAM model [22,23]) for a glass mat-reinforced PP composite. The damage parameters required in the CODAM model were determined through correlations of simulations with the tension, compression and Iosipescu shear experimental results. The simulation with the addition of the shear and compression damage parameters yielded a better prediction than the simulation with assumed shear and compression parameters.

In 2008, Temimi-Maaref et al. [20] developed a phenomenological model based on experimental observations of PP materials under tensile and shear loading conditions, using a unique set of parameters. The prediction of the shear behavior was acceptable, but relevant variations from the experimental curves were observed. Moreover, they concluded that the assumptions of pure elasticity, isotropic damage and isochoricity were invalid.

In 2012, Daiyan et al. [21] analyzed and compared the distribution of shear strain and strain states for two in-plane shear test fixtures (Iosipescu and V-notched rail), using digital image correlation (DIC) and numerical simulations. The investigated materials (non-recycled polymers) were a 20 wt.% TFPP, a 40 wt.% TFPP and an unfilled PP homopolymer (PPH). They conducted an in-depth analysis of the shear behavior in order to obtain reliable data for the calibration of material models. From DIC analysis, they observed that, for small strains (~0.045), PPH material showed a less localized strain in the notch area compared with the TFPP materials. Meanwhile, at large strains (~0.2), the strain distribution appeared to be less localized for 20 wt.% TFPP material. Shear data obtained with the Iosipescu [15] fixture showed a shear modulus of 1.22 GPa, 0.49 GPa and 0.59 GPa for the 40 wt.% TFPP, 20 wt.% TFPP and PPH materials, respectively. In contrast, for the shear stress yield, they obtained 22.3 MPa, 10.8 MPa and 23.1 MPa for the 40 wt.% TFPP, 20 wt.% TFPP and PPH materials, respectively.

In 2021, Tan and Falzon [24] developed a phenomenological model to predict the non-linear hardening behavior of composite laminates (unidirectional carbon fiber-reinforced plastics) under finite deformation. Finite element simulations of shear tests of the composite laminates were conducted to validate this phenomenological model. Good prediction was achieved between the numerical models and experimental results. Despite that, a mismatch of the stress–strain curves in the final regime was present due to the absence of a composite damage model in the crystal model used to capture the large plastic matrix shearing and associated fiber rotations.

In a previous study [25], the authors proposed a new phenomenological model (ICP model) that modified the phenomenological model previously proposed by Zhou and Mallick [26,27] in order to correctly predict the complex tensile behavior of thermoplastic materials including the linear viscoelastic deformation, the non-linear viscoelastic deformation, the yielding, the post-yield strain softening and the post-yield strain hardening. The authors performed a validation activity based on data from the literature for the tensile and compressive behavior of polyether ether ketone (PEEK) and polycarbonate (PC) materials.

The ICP model [25] proved to be accurate and effective in predicting all the phases of the tensile flow stress behavior for the considered materials, across a wide range of strain rates and temperature conditions. A comparison with the most recent phenomenological models showed the better fitting performance of the ICP model [25].

The present paper illustrates that an in-depth analysis of the shear behavior, and consequent modeling, of recycled polymers is necessary to significantly improve knowledge on the mechanical behavior for these materials. Indeed, this work provides experimental data analysis on the shear behavior, at three different test operating temperatures (−40, 23 and 85 °C), of two recycled PP composites (a 30 wt.% TFPP and a 30 wt.% SGFPP) obtained by injection molding using 30% material from post-industrial mechanical shredding. These experimental results have been used to broaden the field of application of the ICP model and thus provide a phenomenological model able to predict the shear behavior for the considered materials at different operating temperatures.

2. Materials and Methods

The materials considered in this study are a 30 wt.% talc-filled recycled PP and a 30 wt.% short glass fiber recycled PP used for car interior applications, such as instrument panels, inner door panels and bumper beams. The materials were produced by injection molding using 30% recycled plastic obtained by post-industrial mechanical shredding. They were provided by Centro Ricerche Fiat (CRF, Stellantis, Turin, Italy). The commercial name of the considered materials has been deliberately omitted because of company policies. The principal mechanical, physical and thermal properties are provided by the supplier of the materials (Table 1).

Table 1. Nominal physical, mechanical and thermal properties of the materials used.

Material	Melt Flow Rate [1] [g/10 min]	Recycled Percentage	Flexural Modulus [2] [MPa]	Tensile Strength [2] [MPa]	Izod Impact Strength [2] (Notched) [kJ/m^2]	Heat Deflection Temperature [3] (HDT)
PP 65.40	9	30%	2350	20	5	63
PP 140.80	4	30%	5500	82	10	142

[1] 230 °C/2.16 kg, [2] 23 °C, [3] (185 N/cm^2).

According to company policies (Stellantis, Turin, Italy) for material characterizations, the materials are named based on the Heat Deflection Temperature (HDT) and Izod properties obtained by internal company tests. The two numbers after "PP", in the material column in Table 1, represent the HDT and Izod values, respectively. Therefore, the recycled 30 wt.% TFPP and the recycled 30 wt.% SGFPP materials considered in this study are identified as PP65.40 and PP140.80, respectively.

The materials were produced by injection molding of material plates (Figure 1) using an Elektron EVO 275 (Milacron, Cincinnati, OH, USA) vertical injection molding machine (CRF, Stellantis, Turin, Italy). The injection molding machine was equipped with a custom 2-plate molding die (Table 1) with an adjustable cross-section.

As explained by Stamopoulos and Gazza [28], to avoid any potential effect of the die walls on the fiber orientation, the material is injected inside a planar cavity and, after the cooling-down process, a 200 × 200 mm square plate is obtained, but only the central part of the plate (130 × 150 mm) is considered for the testing activity. Even if the talc has a globular shape, the same production technique is adopted to obtain as uniform a dispersion of the filler as possible. The specimens are cut in the transversal (Cross-Flow, 90°) direction with respect to the injection flow from the middle of the PP composite plate (Figure 1), so that the direction of the applied force is parallel to the injection flow direction in the notched area. The main injection molding process parameters are reported in Table 2.

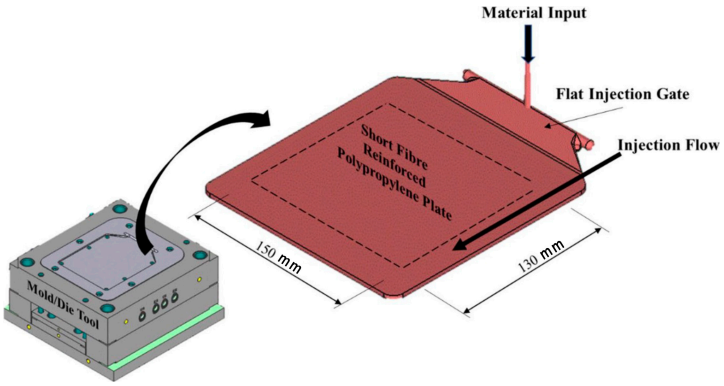

Figure 1. Schematic representation of the dies and the geometry of the injection gate and the resulting composite plate [28].

Table 2. Basic parameters of the injection molding process.

Parameter	Value	Unit
Screw diameter	50	mm
Dosage volume	240	cm^3
Dosage counterpressure	70	bar
Cylinder inner temperature	220	°C
Die inner temperature	35	°C
Speed	145	mm/s
Injection flow	80	cm^3/s
Injection volume	52	cm^3
Commutation pressure	364	bar
Holding pressure	350	bar
Holding time	20	s
Cycle time	62	s

These parameters were chosen based on previous experiences [28] in producing composite plates characterized by a dispersion of the reinforcement as uniform as possible in the central part.

The test method used in this paper is based on the V-Notched Beam Standard (ASTM D5379 [15]) for shear testing, addressing composite materials. Test specimens were machined according to this standard [15], from 4 mm thick injection-molded plates (Figure 1). Figure 2 shows a scheme of the specimen mounted in the testing fixture.

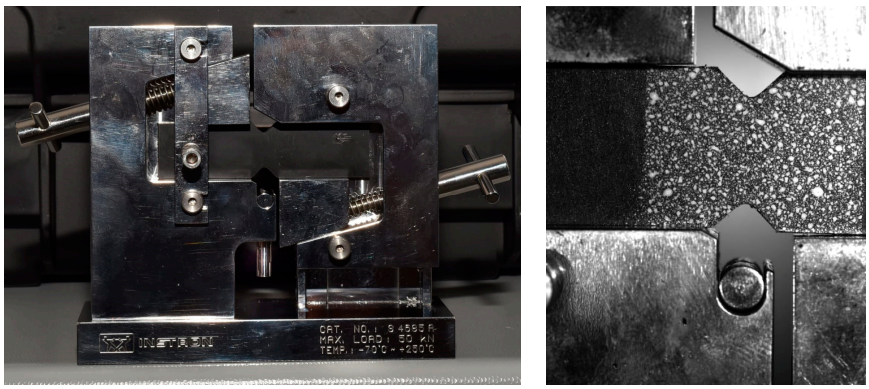

(**a**) (**b**)

Figure 2. Representation of (**a**) the V-Notched Beam Test Fixture and (**b**) a magnification of the notched area of the specimen mounted in the testing fixture during testing.

Shear tests were performed using an MTS Landmark (Eden Prairie, MN, USA), equipped with a 25 kN load cell, provided by the laboratories of the Material Sustainability Engineering Department of Centro Ricerche Fiat (CRF, Stellantis, Turin, Italy). The testing machine was equipped with a LaVision GmbH (Göttingen, Germany) Digital Image Correlation (DIC) system (with DaVis 10 processing software) for the acquisition of the shear strain distribution. Moreover, a Weiss Technik (Hamburg, Germany) climatic chamber was used to perform high-temperature (+85 °C) and low-temperature (−40 °C) tests, pre-conditioning the specimens at the desired temperature before and maintaining a constant temperature during the test. For each test, five specimens were tested and representative curves were considered for the analysis. The temperatures considered in this study are typically used to test materials in the automotive industry [29]. Shear tests were performed at 2 mm/min. According to the ASTM standard D5379 [15], the shear stress (τ), shear strain (γ) and shear chord modulus (G) were determined as described in the calculation section. In particular, the shear strain was computed during the DIC data processing using two virtual orthogonal strain gages centered between the notch roots at ±45°, using Equation (1):

$$\gamma_i = |\varepsilon_{+45,i}| + |\varepsilon_{-45,i}|, \tag{1}$$

where γ_i and $\varepsilon_{\pm 45,i}$ are the engineering shear strain and the normal strain (at ±45°) at the i-th data point, respectively. The ultimate engineering shear strain is determined using Equation (2):

$$\gamma^u = \min\begin{Bmatrix} 5\% \\ \gamma_i \text{ at ultimate load} \end{Bmatrix}. \tag{2}$$

2.1. ICP Model

As more deeply explained in the authors' previous work [25], the proposed ICP constitutive model is based on the formulation proposed by Zhou and Mallick [27]:

$$\sigma = \frac{E(\dot{\varepsilon}, T)\varepsilon}{1 + E(\dot{\varepsilon}, T)\beta(\dot{\varepsilon}, T)\varepsilon^m}. \tag{3}$$

As a result, the Zhou–Mallick model [27] can predict the behavior of a polymer that behaves as a strain-hardening material (when m is less than 1) or as a strain-softening material (when m is greater than 1). When $m = 1$, the slope of the stress–strain diagram becomes zero and the polymer is strain-neutral. The ICP constitutive model [25] was obtained by substituting m in Equation (3) with a polynomial dependent on ε. Therefore, the constitutive equation of the ICP model is expressed as follows:

$$\sigma = \frac{E(\dot{\varepsilon}, T)\varepsilon}{1 + E(\dot{\varepsilon}, T)\ a_0^*(\dot{\varepsilon}, T)\varepsilon^{\sum_{i=0}^{n-1} a_{i+1}(\dot{\varepsilon},T)(\ln \varepsilon)^i}}. \tag{4}$$

When a polynomial degree (n) equal to 1 is imposed, the constitutive equation returns to the original form proposed by Zhou and Mallick [27]:

$$\sigma = \frac{E(\dot{\varepsilon}, T)\varepsilon}{1 + E(\dot{\varepsilon}, T)\ a_0^*(\dot{\varepsilon}, T)\varepsilon^{a_1(\dot{\varepsilon},T)}}, \tag{5}$$

where a_0^* and a_1 are β and m in Equation (3), respectively.

Method to Determine the Parameters in the New Constitutive Equation

In the present paper, the same formulation used for tensile and compressive tests (Equation (4)) was used for the shear test. Therefore, Equation (4) can be rewritten as follows:

$$\tau = \frac{G(\dot{\gamma}, T)\gamma}{1 + G(\dot{\gamma}, T)\ a_0^*(\dot{\gamma}, T)\gamma^{\sum_{i=0}^{n-1} a_{i+1}(\dot{\gamma},T)(\ln \gamma)^i}}, \tag{6}$$

where τ and γ are the shear stress and the shear strain, respectively.

To estimate the parameters $a_0, a_1, \ldots, a_n$ involved in the model, Equation (6) can be rewritten as follows:

$$\frac{\gamma}{\tau} - \frac{1}{G} = a_0^* \gamma^{\sum_{i=0}^{n-1} a_{i+1} (\ln \gamma)^i}, \tag{7}$$

which, by taking natural log on both sides, becomes

$$\ln\left(\frac{\gamma}{\tau} - \frac{1}{G}\right) = \ln(a_0^*) + \left(\sum_{i=0}^{n-1} a_{i+1} (\ln \gamma)^i\right) \ln \gamma. \tag{8}$$

Equation (8) can then be rewritten as follows:

$$\ln\left(\frac{\gamma}{\tau} - \frac{1}{G}\right) = a_0 + \sum_{i=1}^{n} a_i (\ln \gamma)^i, \tag{9}$$

where $a_0 = \ln(a_0^*)$. Finally, Equation (9) can be expressed in a compact form as follows:

$$\ln\left(\frac{\gamma}{\tau} - \frac{1}{G}\right) = \sum_{i=0}^{n} a_i (\ln \gamma)^i. \tag{10}$$

By considering $y = \ln\left(\frac{\gamma}{\tau} - \frac{1}{G}\right)$ and $x = \ln \gamma$, Equation (10) then becomes:

$$y = \sum_{i=0}^{n} a_i x^i. \tag{11}$$

Equation (11) represents a polynomial with degree n. The set of parameter estimates, $\widetilde{\boldsymbol{a}}$, can be obtained from the experimental dataset, (γ_j, τ_j) with $j = 1, \ldots, f$, by applying the Least Squares Method (LSM):

$$\widetilde{\boldsymbol{a}} = \begin{bmatrix} \widetilde{a}_0 \\ \vdots \\ \widetilde{a}_n \end{bmatrix} = (\boldsymbol{X}' \cdot \boldsymbol{X})^{-1} \cdot \boldsymbol{X}' \cdot \boldsymbol{y} \tag{12}$$

being $\boldsymbol{X} = \begin{bmatrix} 1 & \cdots & (\ln \gamma_1)^i \cdots & (\ln \gamma_1)^n \\ \vdots & & \vdots & \vdots \\ 1 & \cdots & \left(\ln \gamma_f\right)^i \cdots & \left(\ln \gamma_f\right)^n \end{bmatrix}$ and $\boldsymbol{y} = \begin{bmatrix} \ln\left(\frac{\gamma_1}{\tau_1} - \frac{1}{G}\right) \\ \vdots \\ \ln\left(\frac{\gamma_f}{\tau_f} - \frac{1}{G}\right) \end{bmatrix}$.

In the present paper, a good fitting for the experimental data was obtained by adopting a polynomial of the 2nd order (n equal to seven in Equation (11)) for the shear behavior of both PP65.40 (Section 3.1.1) and PP140.80 (Section 3.1.2).

The estimation procedure can be repeated for each tested temperature (T). For each testing condition, it is thus possible to estimate a set of parameter estimates, $\widetilde{\boldsymbol{a}}_{\boldsymbol{k}}$ with $k = 1, \ldots, q$. The polynomial function that expresses the variation in the parameter estimates with respect to the testing conditions can be obtained by applying the LSM again. The shape of the polynomial function depends on the number of available testing conditions. In particular, if q testing conditions are available, then q parameters can be estimated at most. In both validation datasets concerning this study (Sections 3.1.1 and 3.1.2), the number of testing conditions is equal to three. Therefore, the polynomial assumed for the i-th estimated parameter, $\widetilde{a}_i$, can be a quadratic model with three parameters:

$$\widetilde{a}_i = \alpha_{i,0} + \alpha_{i,1} T + \alpha_{i,2} T^2. \tag{13}$$

The three parameters $\alpha_{i,0}, \ldots, \alpha_{i,2}$ in Equation (13) can be estimated from the values related to each testing condition, $\left(T_k, \widetilde{a}_{i,k}\right)$ with $k = 1, \ldots, 3$, and by applying the LSM:

$$\widetilde{\boldsymbol{\alpha}}_{\boldsymbol{i}} = \begin{bmatrix} \widetilde{\alpha}_{i,0} \\ \widetilde{\alpha}_{i,1} \\ \widetilde{\alpha}_{i,2} \end{bmatrix} = \left(\boldsymbol{Z}' \cdot \boldsymbol{Z}\right)^{-1} \cdot \boldsymbol{Z}' \cdot \widetilde{\boldsymbol{a}}_{\boldsymbol{i}}, \tag{14}$$

being $\boldsymbol{Z} = \begin{bmatrix} 1 & T_1 & T_1^2 \\ 1 & T_2 & T_2^2 \\ 1 & T_3 & T_3^2 \end{bmatrix}$ and $\widetilde{\boldsymbol{a}}_{\boldsymbol{i}} = \begin{bmatrix} \widetilde{a}_{i,1} \\ \widetilde{a}_{i,2} \\ \widetilde{a}_{i,3} \end{bmatrix}$.

3. Results and Discussion

In this section, data obtained from shear tests of PP65.40 (Section 3.1.1) and PP140.80 (Section 3.1.2) are used to validate and broaden the applicability of the ICP model. Shear tests were conducted across a range of temperatures (−40 °C, 23 °C and 80 °C). Shear chord modulus of elasticity (G) and ultimate shear strength (USS) are computed following the ASTM standard D5379 [15]. In order to evaluate the predictive precision of the ICP model, the coefficient of determination (R^2) is computed for each curve as an index to compare the predicted and experimental curves.

3.1. Shear Tests and Validation of the ICP Model

3.1.1. Recycled 30 wt.% Talc-Filled PP (PP65.40)

The curves in Figure 3 represent the experimental shear stress–strain curves for the recycled 30 wt.% TFPP (PP65.40) material across the three different considered temperatures, and the respective predicted curves using the ICP model.

The experimental curves show different behaviors at different operating temperatures. Indeed, PP65.40 material at −40 °C (Figure 3a) shows brittle behavior and small values of strain at break (3%), as can be shown by the values of the strain compared to the other curves obtained at 23 °C and 80 °C. Meanwhile, tests conducted at 23 °C and 80 °C (Figure 3c) showed a strain-softening behavior and an almost strain-neutral behavior after yielding, respectively, reaching higher values of ultimate shear strain (14% at 23 °C and 18% at 80 °C) compared to the test conducted at −40 °C. Overall, the peak stress decreases, the yielding occurs at higher strain and the ultimate shear strain increases with temperature. The shear chord modulus of elasticity and the ultimate shear strength follow a decreasing trend as the temperature increases, as shown in Table 3.

Table 3. Shear mechanical properties and R^2 values for PP.65.40 material.

Temperature	−40 °C	23 °C	85 °C
G [MPa]	2160.0	1016.7	210.1
USS [MPa]	36.1	17.5	6.0
Shear strain at USS [%]	3.2	14.2	17.7
R^2 [%]	99.96	99.70	99.73

This behavior is probably due to the change in the degree of crystallinity of the polymer. Indeed, the degree of crystallinity of a polymer remains constant below Tg, then it gradually decreases between the Tg and the melting temperature [30], probably resulting from crystal melting. Therefore, a polymer with a larger degree of crystallinity will exhibit a larger drop in mechanical properties between the glass transition point and the rubbery state [31]. The values obtained for G and USS for our recycled 30 wt.% TFPP at 23 °C (Table 3) are comparable with the results obtained for the 40 wt.% and 20 wt.% non-recycled TFPP investigated by Daiyan et al. [21]. Indeed, the G values obtained for our recycled polymer (Table 3) were between 1.22 GPa and 0.49 GPa, which are, respectively, the G values for

the 40 wt.% and 20 wt.% non-recycled TFPP investigated by the authors [21]. Meanwhile, the USS values of our recycled 30 wt.% TFPP at 23 °C (Table 3) were between 22.3 MPa and 10.8 MPa, which are, again, the USS values for the 40 wt.% and 20 wt.% non-recycled TFPP, respectively.

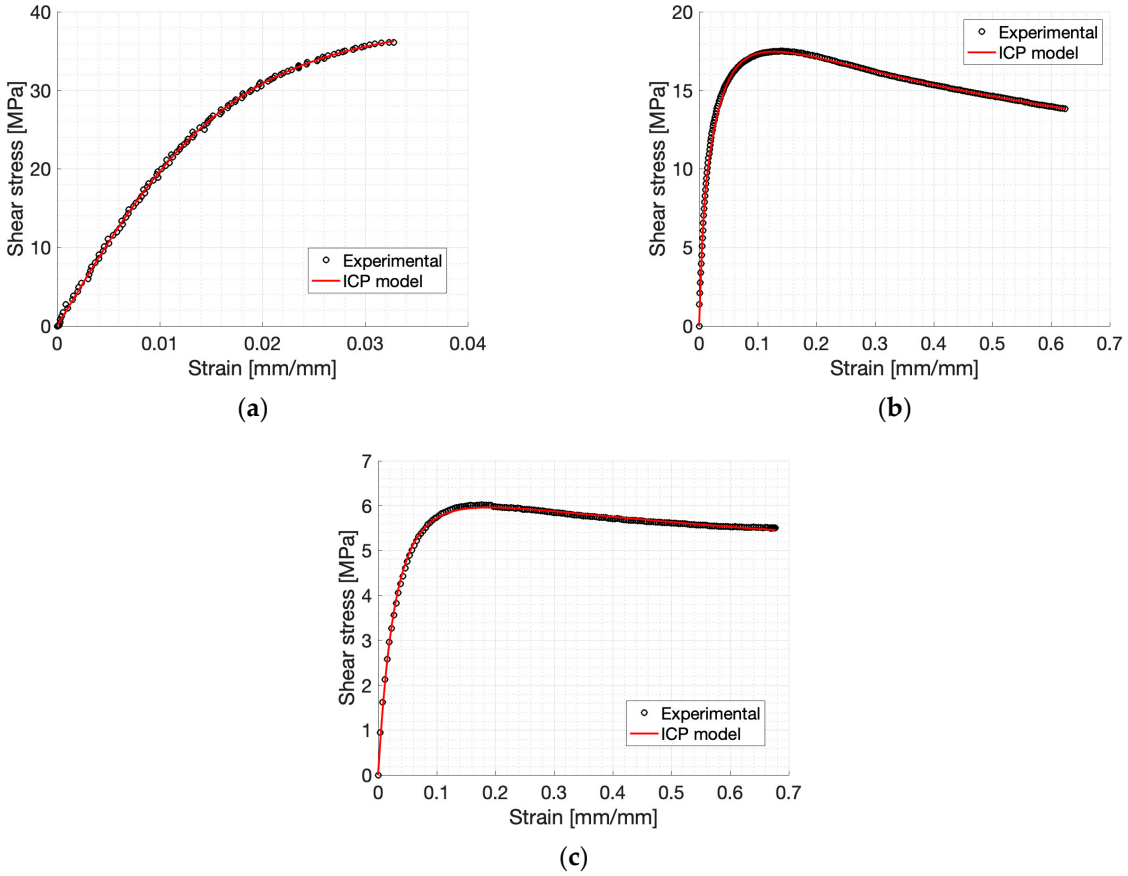

Figure 3. Shear stress–strain curves and predicted results for tensile behavior of PP65.40 at (**a**) −40 °C; (**b**) 23 °C; and (**c**) 85 °C.

Overall, the prediction of the ICP model is precise and accurate and it provides high R^2 values at over 99.7% (Table 3). The curves estimated using the ICP model are in good agreement with the experimental data at all the operating temperatures considered. The proposed model can accurately fit all the phases of the flow stress. The trend, the shape and the peaks of the estimated curves are identical to the experimental ones. The prediction of the curve at 85 °C (Figure 3c) slightly underestimates yielding. To describe the shear behavior of PP65.40 material with the ICP model, a second degree polynomial function was used (Equation (11)). The material coefficients (Equation (14)) needed to implement the model for each temperature are reported in Table 4.

Table 4. Material parameters of the ICP model for the shear behavior of PP65.40.

$\boldsymbol{\alpha_{0,0}}$ $-3.1950 \cdot 10^{0}$	$\boldsymbol{\alpha_{0,1}}$ $3.4643 \cdot 10^{-2}$	$\boldsymbol{\alpha_{0,2}}$ $-1.9739 \cdot 10^{-4}$
$\boldsymbol{\alpha_{1,0}}$ $1.0269 \cdot 10^{0}$	$\boldsymbol{\alpha_{1,1}}$ $1.7593 \cdot 10^{-2}$	$\boldsymbol{\alpha_{1,2}}$ $-1.8992 \cdot 10^{-4}$
$\boldsymbol{\alpha_{2,0}}$ $-2.1017 \cdot 10^{-2}$	$\boldsymbol{\alpha_{2,1}}$ $3.7160 \cdot 10^{-3}$	$\boldsymbol{\alpha_{2,2}}$ $-4.1877 \cdot 10^{-5}$

Therefore, the proposed model can be used to effectively describe the shear behavior of a recycled 30 wt.% TFPP material across different temperatures.

3.1.2. Recycled 30 wt.% Short Glass Fiber-Reinforced PP (PP140.80)

The curves in Figure 4 represent the experimental shear stress–strain curves for the recycled 30 wt.% SGFPP (PP140.80) material across the three temperatures considered, and the respective predicted curves using the ICP model.

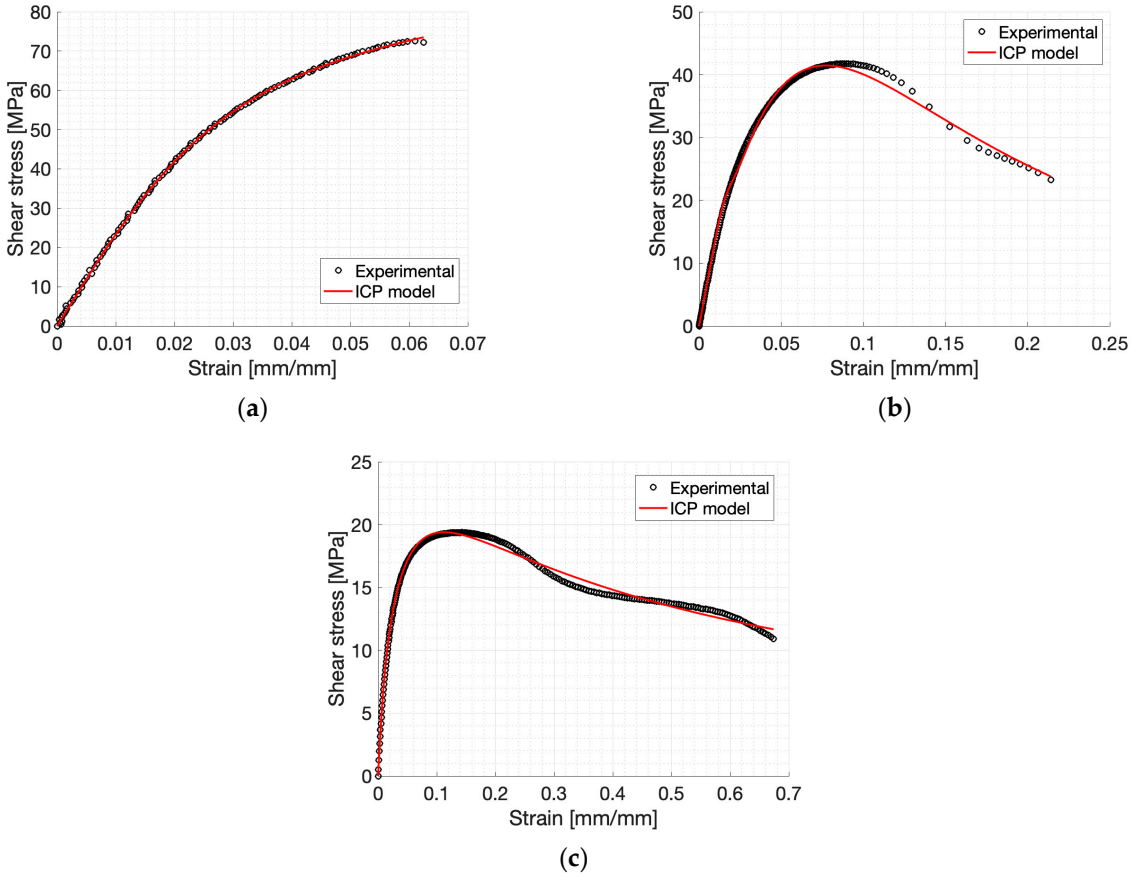

Figure 4. Shear stress–strain curves and predicted results for tensile behavior of PP140.80 at (**a**) −40 °C; (**b**) 23 °C; and (**c**) 85 °C.

The shear behavior of PP140.80 and PP65.40 materials is similar across the different operating temperatures. As for PP65.40 material, PP140.80 at −40 °C (Figure 4a) shows a more brittle behavior and smaller values of strain at break (6%). Tests conducted at 23 °C and 80 °C (Figure 4b,c) showed strain-softening behavior with ultimate shear strain of 9% and 14%, respectively. Overall, the peak stress decreases, as also reported in Table 5, the yielding points move rightwards at higher strains and the ultimate shear strain is larger as the temperature increases.

Table 5. Shear mechanical properties and R^2 values for PP140.80 material.

Temperature	**−40 °C**	**23 °C**	**85 °C**
G [MPa]	2386.0	1393.1	908.0
USS [MPa]	72.5	41.8	19.4
Shear strain at USS [%]	6.10	8.8	14.3
R^2 [%]	99.97	99.75	99.31

The shear chord modulus of elasticity and ultimate shear strength obtained for PP140.80 are higher compared to PP65.40 material due to the different types, sizes and shapes of the reinforcement. However, the results show a similar decreasing trend with tem-

perature, as reported in Table 5. Moreover, a comparison of the shear properties between PP65.40 (Section 3.1.1) and PP140.80 materials is reported in Table 6.

Table 6. Increment for PP140.80 material of G and USS properties with respect to PP65.40 material.

Temperature	−40 °C	23 °C	85 °C
G [MPa]	+10%	+37%	+332%
USS [MPa]	+101%	+139%	+223%

The results show that the G values for the recycled 30 wt.% SGFPP are higher than those of the recycled 30 wt.% TFPP at about 10% in the case of −40 °C. This increment becomes larger at room operating temperature (23 °C) and, at 85 °C, PP140.80 material shows a G value more than three times larger with respect to PP65.40 material. This increasing trend is also exhibited by the USS values (Table 6). Indeed, the increments are all above 100%, and they increase with temperature from almost 100% increment at −40 °C to more than 200% increment at 85 °C.

Again, the prediction of the ICP model is precise and accurate and gives very good R^2 values (Table 5). The curves estimated using the ICP model are in good agreement with the experimental data at all the operating temperatures considered. The proposed model can fit all the phases of the flow stress. The trend and the peaks of the estimated curves are very close to the experimental ones. The prediction of the curves at 23 °C and 80 °C (Figure 4b,c) anticipates the yielding behavior and the shape of the post-yielding behavior is not well captured. As for PP65.40, to describe the shear behavior of PP140.80 material with the ICP model, a second degree polynomial function was used (Equation (11)). The material coefficients (Equation (14)) needed to implement the model for each temperature are reported in Table 7.

Table 7. Material parameters of the ICP model for the shear behavior of PP140.80.

$\alpha_{0,0}$	$\alpha_{0,1}$	$\alpha_{0,2}$
$-1.7608 \cdot 10^{0}$	$7.1996 \cdot 10^{-2}$	$-9.1440 \cdot 10^{-4}$
$\alpha_{1,0}$	$\alpha_{1,1}$	$\alpha_{1,2}$
$2.5408E \cdot 10^{0}$	$4.3516 \cdot 10^{-2}$	$-6.4020 \cdot 10^{-4}$
$\alpha_{2,0}$	$\alpha_{2,1}$	$\alpha_{2,2}$
$1.8445 \cdot 10^{-1}$	$7.7825 \cdot 10^{-3}$	$-1.0510 \cdot 10^{-4}$

Therefore, the proposed model can be used to effectively describe the shear behavior of a recycled 30 wt.% SGFPP material across different operating temperatures.

As shown in Figure 5, it is also possible to increase the polynomial degree in Equation (11) for PP140.80 material at 23 °C (Figure 4b) and 85 °C (Figure 4c) in order to better describe the shear behavior of these materials using the ICP model.

Polynomials with 8 and 9 degrees (Equation (11)) can be adopted to improve the prediction of the shear behavior of PP140.80 material at 23 °C (Figure 5a) and 85 °C (Figure 5b), respectively. By increasing the polynomial degree in Equation (11), the number of parameter estimates using Equation (12) increases, as shown in Tables 8 and 9, and so does the complexity of the ICP model.

Table 8. Set of parameter estimates for PP140.80 material at 23 °C considering an 8th-degree polynomial function.

a_0	a_1	a_2
$-1.925 \cdot 10^{1}$	$-1.149 \cdot 10^{1}$	$1.331 \cdot 10^{1}$
a_3	a_4	a_5
$7.761 \cdot 10^{0}$	$-1.365 \cdot 10^{1}$	$-1.514 \cdot 10^{1}$
a_6	a_7	a_8
$-6.125 \cdot 10^{0}$	$-1.145 \cdot 10^{0}$	$-8.292 \cdot 10^{-2}$

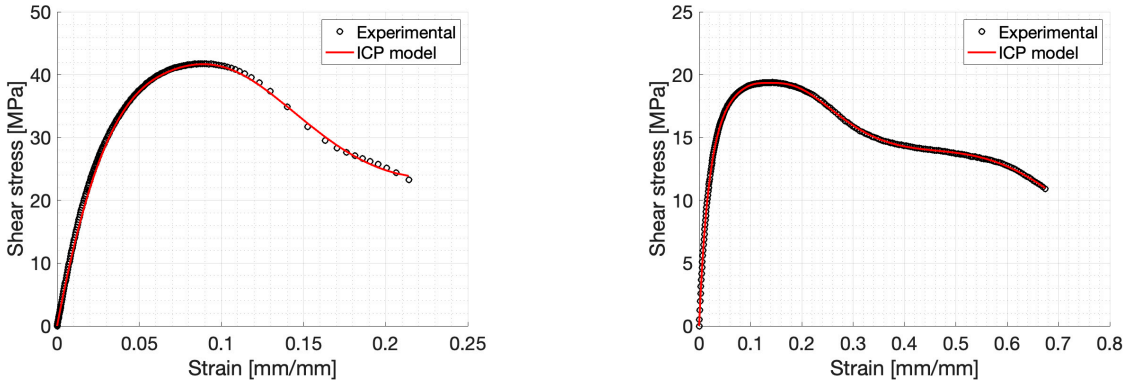

Figure 5. Shear stress–strain curves and optimized predicted results for tensile behavior of PP140.80 at (**a**) 23 °C, adopting an 8th-degree polynomial and (**b**) 85 °C, adopting a 9th-degree polynomial.

Table 9. Set of parameter estimates for PP140.80 material at 85 °C considering a 9th-degree polynomial function.

a_0	a_1	a_2	a_3	a_4
$-7.2545 \cdot 10^{-1}$	$8.1965 \cdot 10^{0}$	$7.6972 \cdot 10^{0}$	$-1.4753 \cdot 10^{0}$	$-6.1061 \cdot 10^{0}$
a_5	a_6	a_7	a_8	a_9
$6.9562 \cdot 10^{-1}$	$5.7093 \cdot 10^{0}$	$3.8304 \cdot 10^{0}$	$1.0524 \cdot 10^{0}$	$1.0774 \cdot 10^{-1}$

A higher degree of polynomial function provides better R^2 values (Table 10) compared to those obtained using a second degree polynomial function (Table 5). With more parameters (Tables 8 and 9), the model can better fit all the phases of the flow stress.

Table 10. R^2 values for PP140.80 material at 23 °C and 85 °C considering higher degree of polynomial function.

Temperature	**23 °C**	**85 °C**
Polynomial degree (*n*)	8	9
R^2 [%]	99.79	99.96

Therefore, a second degree polynomial function is enough to obtain an effective prediction of the experimental curves (Figure 4) for all the materials and the operating temperatures considered. On the other hand, to obtain a more precise and accurate prediction for a particular case or loading condition, it could be useful to increase the polynomial degree at the expense of a higher model complexity.

4. Conclusions

In the present paper, shear tests using the Iosipescu testing apparatus (ASTM D5379 [15]) were performed at three different operating temperatures (−40, 23 and 85 °C) for a recycled 30 wt.% short glass fiber-reinforced polypropylene (PP140.80) and a recycled 30 wt.% talc-filled polypropylene (PP65.40).

The shear chord modulus (G) and the ultimate shear strength (USS) values obtained from the shear tests of PP65.40 and PP140.80 showed similar trends across the considered operating temperatures. Indeed, the peak stress decreases with temperature and the yielding behavior occurs at higher strain by increasing the operating temperature for both materials. The values of G and USS obtained for PP140.80 are higher compared to PP65.40 material for all the temperatures considered, and the gap is larger as the temperature increases (Table 6).

To accurately describe the shear behavior of both PP65.40 and PP140.80, a second degree polynomial function of the ICP constitutive equation (Equation (11), Section: Method

to Determine the Parameters in the New Constitutive Equation) is required. The lower the polynomial degree, the lower the number of material coefficients (Equation (14), Section: Method to Determine the Parameters in the New Constitutive Equation) present in the proposed model, thus reducing its complexity. Higher accuracy can be obtained by increasing the degree of the polynomial function in the ICP constitutive equation.

The proposed ICP model shows good agreement with the experimental curves, thus resulting in it being suitable for predicting the shear behavior of a 30 wt.% short glass fiber and a 30 wt.% talc-filled recycled polypropylene with a very high level of accuracy across the range of temperatures considered.

This research has highlighted the possibility of using recycled polymers, which have shown comparable mechanical properties to similar non-recycled plastics, and the possibility of also applying the previously developed ICP model for predicting the shear behavior of polypropylene composites in order to condense, into a limited number of parameters, the trend of the curves that can be obtained at different temperature levels.

Further studies on different materials (i.e., thermosetting polymers, rubbery thermoplastics, composites) and different loading conditions (i.e., torsion, bending) should be performed to further broaden the field of application of the ICP model.

Author Contributions: Conceptualization, A.I., R.C. and D.S.P.; methodology, A.I., R.C. and D.S.P.; software, A.I.; validation, A.I., R.C. and D.S.P.; formal analysis, A.I.; investigation, A.I. and P.D.M.; resources, A.I.; data curation, A.I. and R.C.; writing—original draft preparation, A.I.; writing—review and editing, A.I., R.C. and D.S.P.; visualization, A.I. and R.C.; supervision, D.S.P.; project administration, D.S.P., V.B., F.G. and V.G.L. All authors have read and agreed to the published version of the manuscript.

Funding: This research received no external funding.

Data Availability Statement: The data presented in this study are available on request from the corresponding author. (The data are not publicly available due to privacy or ethical restrictions.).

Acknowledgments: The authors acknowledge support and instrumentation offered by Cenro Ricerche Fiat (CRF, Stellantis, Turin, Italy).

Conflicts of Interest: Authors Francesco Gazza and Vito Guido Lambertini were employed by Materials Technical Expertise, Centro Ricerche Fiat (Stellantis). The remaining authors declare that the research was conducted in the absence of any commercial or financial relationships that could be construed as potential conflicts of interest.

References

1. Maxwell, J. *Plastics in the Automotive Industry*, 1st ed.; Woodhead Publishing: Cambridge, UK, 1994.
2. Ciardiello, R. The mechanical performance of re-bonded and healed adhesive joints activable through induction heating systems. *Materials* **2021**, *14*, 6351. [CrossRef] [PubMed]
3. Mohammadi, H.; Ahmad, Z.; Mazlan, S.A.; Johari, M.A.F.; Siebert, G.; Petrů, M.; Koloor, S.S.R. Lightweight Glass Fiber-Reinforced Polymer Composite for Automotive Bumper Applications: A Review. *Ploymers* **2023**, *15*, 193. [CrossRef] [PubMed]
4. Niessner, N. *Recycling of Plastics*; Carl Hanser Verlag GmbH & Co., KG: München, Germany, 2023. [CrossRef]
5. Kooduvalli, K.; Unser, J.; Ozcan, S.; Vaidya, U.K. Embodied Energy in Pyrolysis and Solvolysis Approaches to Recycling for Carbon Fiber-Epoxy Reinforced Composite Waste Streams. *Recycling* **2022**, *7*, 6. [CrossRef]
6. Cheng, S.; Wong, K.H.; Shen, C.P.; Liu, X.L.; Rudd, C. Shredding energy consumption of GFRP composite waste. *J. Phys. Conf. Ser.* **2021**, *1765*, 012015. [CrossRef]
7. Gonçalves, R.M.; Martinho, A.; Oliveira, J.P. Recycling of Reinforced Glass Fibers Waste: Current Status. *Materials* **2022**, *15*, 1596. [CrossRef]
8. Vaidya, U.; Wasti, S.; Tekinalp, H.; Hassen, A.A.; Ozcan, S. Recycled Glass Polypropylene Composites from Transportation Manufacturing Waste. *J. Compos. Sci.* **2023**, *7*, 99. [CrossRef]
9. Ramsteiner, F.; Theysohn, R. The Influence of Fibre Diameter on the Tensile Behaviour of Short-glass-fibre Reinforced Polymers. *Compos. Sci. Technol.* **1985**, *24*, 231–240. [CrossRef]
10. Mortazavian, S.; Fatemi, A. Effects of fiber orientation and anisotropy on tensile strength and elastic modulus of short fiber reinforced polymer composites. *Compos. B Eng.* **2015**, *72*, 116–129. [CrossRef]
11. Farooque, R.; Asjad, M.; Rizvi, S. A current state of art applied to injection moulding manufacturing process—A review. *Mater. Today Proc.* **2020**, *43*, 441–446. [CrossRef]

12. Mortazavian, S.; Fatemi, A. Tensile behavior and modeling of short fiber-reinforced polymer composites including temperature and strain rate effects. *J. Thermoplast. Compos. Mater.* **2017**, *30*, 1414–1437. [CrossRef]
13. Wang, Z.; Zhou, Y.; Mallick, P.K. Effects of Temperature and Strain Rate on the Tensile Behavior of Short Fiber Reinforced Polyamide-6. *Polym. Compos.* **2002**, *23*, 858–871. [CrossRef]
14. G'Sell, C.; Boni, S.; Shrivastava, S. Application of the plane simple shear test for determination of the plastic behaviour of solid polymers at large strains. *J. Mater. Sci.* **1983**, *18*, 903–918. [CrossRef]
15. *D5379/D5379M*; Standard Test Method for Shear Properties of Composite Materials by the V-Notched Beam Method. ASTM International: West Conshohocken, PA, USA, 2019. [CrossRef]
16. Weinberg, M. Shear testing of neat thermoplastic resins and their unidirectional graphite composites. *Composites* **1987**, *18*, 386–392. [CrossRef]
17. Codolini, A.; Li, Q.; Wilkinson, A. Mechanical characterization of thin injection-moulded polypropylene specimens under large in-plane shear deformations. *Polym. Test.* **2018**, *69*, 485–489. [CrossRef]
18. Xiang, C.; Sue, H.-J. Iosipescu shear deformation and fracture in model thermoplastic polyolefins. *J. Appl. Polym. Sci.* **2001**, *82*, 3201–3214. [CrossRef]
19. Xiao, X. Evaluation of a composite damage constitutive model for PP composites. *Compos. Struct.* **2007**, *79*, 163–173. [CrossRef]
20. Temimi-Maaref, N.; Burr, A.; Billon, N. Damaging processes in polypropylene compound: Experiment and modeling. *Polym. Sci. Ser. A* **2008**, *50*, 558–567. [CrossRef]
21. Daiyan, H.; Andreassen, E.; Grytten, F.; Osnes, H.; Gaarder, R.H. Shear Testing of Polypropylene Materials Analysed by Digital Image Correlation and Numerical Simulations. *Exp. Mech.* **2012**, *52*, 1355–1369. [CrossRef]
22. Williams, K.V.; Vaziri, R. Application of a damage mechanics model for predicting the impact response of composite materials. *Comput. Struct.* **2001**, *79*, 997–1011. Available online: www.elsevier.com/locate/compstruc (accessed on 5 June 2024). [CrossRef]
23. Williams, K.V.; Vaziri, R.; Poursartip, A. A physically based continuum damage mechanics model for thin laminated composite structures. *Int. J. Solids Struct.* **2003**, *40*, 2267–2300. [CrossRef]
24. Tan, W.; Falzon, B.G. A crystal plasticity phenomenological model to capture the non-linear shear response of carbon fibre reinforced composites. *Int. J. Lightweight Mater. Manuf.* **2021**, *4*, 99–109. [CrossRef]
25. Iadarola, A.; Ciardiello, R.; Paolino, D.S. A new effective phenomenological constitutive model for semi-crystalline and amorphous polymers. *Polym. Eng. Sci.* **2024**, *64*, 3730–3750. [CrossRef]
26. Zhou, Y.; Mallick, P.K. Effects of temperature and strain rate on the tensile behavior of unfilled and talc-filled polypropylene. Part I: Experiments. *Polym. Eng. Sci.* **2002**, *42*, 2449–2460. [CrossRef]
27. YZhou, Y.; Mallick, P.K. Effects of temperature and strain rate on the tensile behavior of unfilled and talc-filled polypropylene. Part II: Constitutive equation. *Polym. Eng. Sci.* **2002**, *42*, 2461–2470. [CrossRef]
28. Stamopoulos, A.G.; Gazza, F.; Neirotti, G. Assessment of the compressive mechanical behavior of injection molded E-glass/polypropylene by mechanical testing and X-ray computed tomography. *Int. J. Adv. Manuf. Technol.* **2023**, *126*, 209–223. [CrossRef]
29. Ciardiello, R.; Belingardi, G.; Martorana, B.; Brunella, V. Effect Of Accelerated Ageing Cycles on the Physical And Mechanical Properties of a Reversible Thermoplastic Adhesive. *J. Adhes.* **2020**, *96*, 1003–1026. [CrossRef]
30. Lin, Y.; Li, X.; Meng, L.; Chen, X.; Lv, F.; Zhang, Q.; Zhang, R.; Li, L. Structural Evolution of Hard-Elastic Isotactic Polypropylene Film during Uniaxial Tensile Deformation: The Effect of Temperature. *Macromolecules* **2018**, *51*, 2690–2705. [CrossRef]
31. Huang, P.-Y.; Guo, Z.-S.; Feng, J.-M. General Model of Temperature-dependent Modulus and Yield Strength of Thermoplastic Polymers. *Chin. J. Polym. Sci. (Engl. Ed.)* **2020**, *38*, 382–393. [CrossRef]